17. M. Mann, C. K. Meng, J. B. Fenn, *Anal. Chem.* **61**, 1702 (1989).
18. J. A. Loo and R. Pesch, *ibid.* **66**, 3659 (1994); M. R. Emmett and R. M. Caprioli, *J. Am. Soc. Mass Spectrom.* **5**, 605 (1994).
19. Fresh human blood (5 μl) that should contain ≈200 pmol of CA [R. B. Pennell, in *The Red Blood Cell*, D. N. Surgenor, Ed. (Academic Press, New York, 1974), vol. 1, pp. 93–105] was extracted with methanol–water–carbon tetrachloride [S. Lindskog, *Biochim. Biophys. Acta* **39**, 218 (1960); ≈80% efficiency] without electrophoretic purification; the aqueous layer was desalted twice (≈95% efficiency each) by ultrafiltration (10 kD), the retentate was diluted (10 mM acetic acid) to 400 μl, and 18 pl was injected.
20. K. T. Flaming and D. G. Brown, *Advanced Micropipette Techniques for Cell Physiology* (Wiley-Interscience, Chichester, 1986); B. Sakmann and E. Neher, Eds., *Single-Channel Recording* (Plenum, New York, 1983).
21. A nonredundant database is maintained by C. Sanders at EMBL and can be downloaded by FTP from ebi.ac.uk/pub/databases/Peptidesearch.
22. E. Mørtz *et al.*, *Proc. Natl. Acad. Sci. U.S.A.* **93**, 8264 (1996).
23. N. L. Kelleher, C. A. Costello, T. P. Begley, F. W. McLafferty, *J. Am. Soc. Mass Spectrom.* **6**, 981 (1995); J. P. Speir, M. W. Senko, D. P. Little, J. A. Loo, F. W. McLafferty, *J. Mass Spectrom.* **30**, 39 (1995).
24. J. A. Loo, C. G. Edmonds, R. D. Smith, *Anal. Chem.* **63**, 2488 (1991).
25. P. Roepstorff and J. Fohlman, *Biomed. Mass Spectrom.* **11**, 601 (1984).
26. M. Mann and M. Wilm, *Anal. Chem.* **66**, 4390 (1994).
27. S. A. Hofstadler, J. H. Wahl, J. E. Bruce, R. D. Smith, *J. Am. Chem. Soc.* **115**, 6983 (1993).
28. R. F. Curl and R. E. Smalley, *Science* **242**, 1017 (1988).
29. D. P. Little, D. J. Aaserud, G. A. Valaskovic, F. W. McLafferty, *J. Am. Chem. Soc.*, in press.
30. We thank D. J. Aaserud, Z. Guan, E. K. Fridriksson, H. Lin, T. D. Wood, and M. W. Senko for advice and experimental assistance and G. H. Morrison and M. Holton for tip fabrication equipment. This work was supported under NIH grant GM16609 (to F.W.M.) and cell and molecular biology training grant 08-T2GM07273 (to N.L.K.).

7 May 1996; accepted 16 July 1996

Postseismic Rebound in Fault Step-Overs Caused by Pore Fluid Flow

Gilles Peltzer, Paul Rosen, Francois Rogez, Ken Hudnut

Near-field strain induced by large crustal earthquakes results in changes in pore fluid pressure that dissipate with time and produce surface deformation. Synthetic aperture radar (SAR) interferometry revealed several centimeters of postseismic uplift in pull-apart structures and subsidence in a compressive jog along the Landers, California, 1992 earthquake surface rupture, with a relaxation time of 270 ± 45 days. Such a postseismic rebound may be explained by the transition of the Poisson's ratio of the deformed volumes of rock from undrained to drained conditions as pore fluid flow allows pore pressure to return to hydrostatic equilibrium.

Large earthquakes are followed by slow transient deformations of the crust over days to years. Over large areas, this deformation is generally thought to be caused by the viscous response of the lower crust and upper mantle to the faulting in the brittle crust (*1*). Pore fluid flow has also been proposed to explain aftershock activity (*2*), cross-fault triggering of earthquakes (*3*), and shallow postseismic movements (*4*) with typical decay times of several months to a few years. Surface deformation patterns associated with shallow processes are of small spatial extent and are thus difficult to detect using conventional geodetic techniques (*5*). Here, we used the technique of SAR interferometry (*6*) to analyze postseismic surface displacement in the near field of the 1992 Landers, California, earthquake rupture.

To map postseismic displacement, we combined SAR images spanning three different time intervals in the 3 years after the earthquake (*7*). The interferogram shown in Fig. 1 covers 41 days after the event, starting on 7 August 1992. The most striking features are the localized strain along three sections of the 1992 surface rupture, where the rupture changed direction or jumped to another fault branch and formed two pull-apart structures and a compressive jog (boxes in Fig. 1) (*8*).

The first zone of high strain is where the Emerson fault connects with the Camp Rock fault. The southern fault branch bends westerly and a smaller surface break steps slightly to the east. The westerly-bending branch accommodated most of the displacement (*9*), making it a compressive jog along the overall right-lateral fault. The local compressive regime resulted in coseismic vertical offsets of up to 1 m along the bent section of the main rupture (*9*). The postseismic displacement near this section of the fault produced a range increase in the radar interferogram (profile 1, Figs. 1 and 2).

The second zone of high strain is localized in a pull-apart structure between the overlapping sections of the Homestead Valley and Emerson faults. During the earthquake, the volume of rock in the pull-apart accommodated extension while transferring ~3.5 m of slip from the Homestead Valley fault in the south into ~4.5 m of right-lateral slip on the Emerson fault in the north (*9*). The postseismic surface displacement observed across this zone produced a range decrease in the radar data (Figs. 1 and 2).

The third zone of high strain is observed in the step-over between the Homestead Valley and Johnson Valley faults. The Kickapoo fault connects these two overlapping faults across the pull-apart and accommodated a part of the 3.3 m of coseismic horizontal slip while slip was progressively transferred from the Johnson Valley fault in the south to the Homestead Valley fault in the north (*10*). Many surface breaks were seen near the Homestead Valley fault and east of the Kickapoo fault (*10*). Leveling data across the Homestead Valley–Kickapoo–Johnson Valley faults indicate that the basin between the faults subsided by ~20 cm between 1979 and 1994 (*11*). Although this time interval covers 15 years, including 1.5 years of postseismic period, it is likely that subsidence of a few tens of centimeters occurred during the 1992 earthquake. The postseismic displacement of the ground across the fault step-over produced a range decrease in the radar data (Figs. 1 and 2).

Radar interferograms provide estimates of the component of the ground displacement parallel to the satellite line of sight (*12*). Independent observations are needed to derive the actual displacement of the ground. In all of the cases described above, we interpret the phase changes as being produced by vertical motion of the ground for the following reasons. Zones of high strain are observed only in fault step-overs, or where the faulting changed direction (that is, in regions characterized by a component of vertical displacement during the earthquake as a result of local compression or extension). Postseismic vertical adjustments are thus likely to occur in these regions. Moreover, the profile of section 3 (from west to east) shows a steep range decrease across the Johnson Valley fault and a steep range increase across the Homestead Valley fault; the zone between shows a relatively flat phase offset with respect to the far field on both sides (Fig. 2). If such range changes were caused by horizontal motion, equal magnitudes of right-lateral slip across the Johnson Valley fault and left-lateral slip across the Homestead Valley fault would be required because the profiles do not show any far-field offset. In other

G. Peltzer, P. Rosen, F. Rogez, Jet Propulsion Laboratory, 4800 Oak Grove Drive, Pasadena, CA 91109, USA.
K. Hudnut, U.S. Geological Survey, Pasadena, CA 91125, USA.

words, the block between the two faults would have to have moved rigidly to the south. Such a possibility is rather unlikely.

An interpretation of the observed signal as a result of vertical motion implies that the volumes of rock that experienced dilation or compression during the earthquake underwent additional postseismic deformation that produced vertical displacement of the surface. In the three zones described above, postseismic deformation resulted in upheaval where the coseismic stress regime was locally extensive and subsidence where the coseismic stress regime was locally compressive.

The mechanism responsible for the surface movements observed in the fault stepovers appears to occur at a rate that decays exponentially with time. The profiles in Fig. 2 that show the largest displacement correspond to the time interval starting 41 days after the earthquake, earlier than the two other time intervals covered by the radar data. The longest time interval covers a period of 3.4 years starting 92 days after the earthquake, yet the observed displacement during this interval is ~20% smaller than the displacement observed in the earliest interval (Fig. 2). We thus assume that the postseismic surface displacement w varies with time according to

$$w = w_0[1 - \exp(-t/\tau)] \quad (1)$$

where t is time since the earthquake, τ is the relaxation time, and w_0 is the vertical adjustment after an infinite time. From the displacement profiles, we can measure the finite vertical displacement Δw_i that occurred during the interval i defined by starting time t_i and ending time s_i (i = 1, 2, 3). According to Eq. 1, Δw_i follows

$$w_0[\exp(-t_i/\tau) - \exp(-s_i/\tau)] = \Delta w_i + \sigma_i \quad (2)$$

where σ_i is the error in the estimate of Δw_i. Estimates of τ and w_0 can be obtained by minimizing the weighted sum of squared differences between observed and modeled displacements. Using profiles of section 3 (Fig. 2), we measured average surface uplifts of 4.9, 3.9, and 2.8 cm (error, ±0.5 cm) for the three time intervals sampled by the radar data. These data give a relaxation time τ = 273 ± 44 days and a maximum displacement w_0 = 6.2 ± 0.5 cm. Such a relaxation time is almost an order of magnitude greater than the relaxation time of 34 days derived from the Global Positioning System (GPS) data; this finding suggests that the process responsible for the observed vertical rebound in the fault stepovers is not governed by viscous flow of the lower crust, which has often been proposed to explain deep fault after-slip (1). However, relaxation times of hundreds of days are characteristic of postseismic phenomena that are often explained by pore fluid flow in the upper crust (2, 4, 13, 14).

A simple model shows that pore fluid transfer could produce uplift or subsidence of the surface after an earthquake by up to several centimeters in places where coseismic strain involves compression or dilation. If rocks in a pull-apart deform homogeneously to accommodate the slip transferred across the pull-apart, the extensional strain parallel to the direction of the fault is $\varepsilon_1 = \delta l/l$, where δl is the amount of transferred fault slip and l is the distance over which the faults overlap. For simplicity, we assume that deformation is accommodated by plane strain parallel to the fault. If the Poisson's ratio of the volume of rock is ν, the vertical strain accommodated by the block is $\varepsilon_2 = \nu\varepsilon_1$. If we neglect any isostatic adjustment, the associated subsidence of the surface is $\delta z = \varepsilon_2 h$, where h is the thickness of the block. Because coseismic stress changes are rapid relative to the fluid diffusion time, at short times after an earthquake, the volume of rock is deformed under undrained conditions. The coseismic subsidence in the pull-apart is therefore

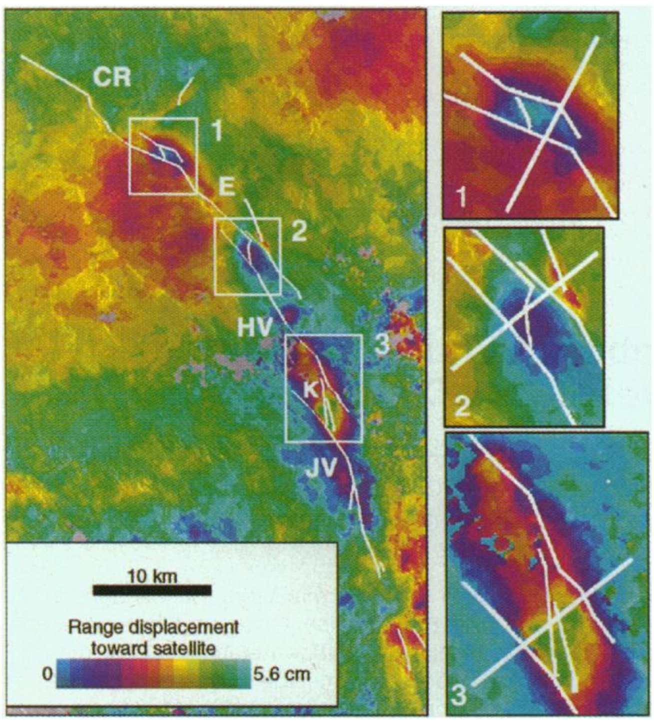

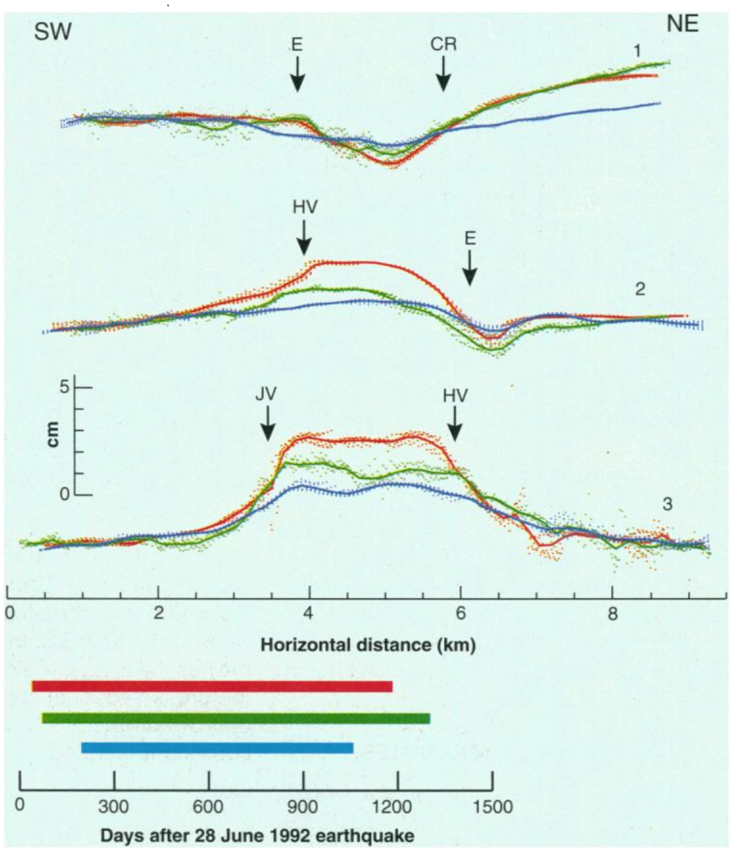

Fig. 1 (left). Three-pass interferogram of the Landers area generated with SAR image triplet A (7). White line depicts 1992 surface rupture. Straight lines in zoomed areas are profiles shown in Fig. 2. Fault labels: CR, Camp Rock fault; E, Emerson fault; K, Kickapoo fault; JV, Johnson Valley fault; and HV, Homestead Valley fault. **Fig. 2 (right).** Line-of-sight surface displacement along profiles 1, 2, and 3 shown in Fig. 1 for interferograms A (red; from 7 August 1992 to 24 September 1995), B (green; from 27 September 1992 to 23 January 1996), and C (blue; from 10 January 1993 to 23 May 1995) (7). Dots represent displacement of individual image pixels within ~400 m of the profile line; solid curves indicate values averaged in bins (length ~160 m) along the profile strike. Fault labels are as in Fig. 1. The vertical scale is the slant range displacement toward the satellite.

$$\delta z_u = \nu_u \varepsilon_1 h \quad (3)$$

where ν_u is the Poisson's ratio of the undrained material. As time proceeds and the pore pressure gradients caused by the earthquake are dissipated, the volume of rock will eventually reach a drained state. The residual subsidence after complete hydrostatic re-equilibrium of pore pressure is

$$\delta z_d = \nu_d \varepsilon_1 h \quad (4)$$

where ν_d is the Poisson's ratio of the drained material. Because ν_u is larger than ν_d (*15*), postseismic adjustment of pore pressure in the pull-apart results in surface upheaval

$$u = (\nu_u - \nu_d)\varepsilon_1 h \quad (5)$$

Conversely, if coseismic strain produced local compression of a volume of rock, the coseismic deformation would produce uplift and the postseismic flow of pore fluid would cause subsidence. Such a process would explain the observed subsidence in the restraining bend along the Emerson fault (profile 1, Figs. 1 and 2).

Typical values for the Poisson's ratios of drained and undrained materials yield $\nu_u - \nu_d = 0.03$ (*15*). Assuming that $\delta l = 3$ m [as estimated across the Homestead Valley pull-apart (*10*)], $l = 5$ km, and $h = 4$ km, Eq. 5 gives a postseismic uplift $u = 7$ cm. The amount of uplift increases linearly with the porosity and thickness of the layer and decreases as the Poisson's ratio of the pristine rock increases, such that a trade-off exists between these parameters. However, the calculation shows that the use of reasonable values for these parameters yields a few centimeters of postseismic uplift, consistent with the radar data.

We thus conclude that pore fluid transfer provides a plausible mechanism to account for postseismic rebound in fault step-overs. Our model accounts both for postseismic subsidence in compressive jogs and uplift in pull-apart structures (*16*). The relaxation times involved in pore fluid flow processes (*2, 17*) and the modeled amplitude of vertical surface adjustments are consistent with the observed decay rate and amplitude of postseismic surface movements in the step-overs of the 1992 Landers break. A critical test of this model would require pore pressure data that can be obtained by water-level measurement in wells near rupture zones. Such data are lacking in the region of Landers.

REFERENCES AND NOTES

1. For example, see Z. K. Shen *et al.*, *Bull. Seismol. Soc. Am.* **84**, 780 (1994); F. K. Wyatt, D. C. Agnew, M. Gladwin, *ibid.*, p. 768.
2. A. Nur and J. R. Booker, *Science* **175**, 885 (1972).
3. K. W. Hudnut, L. Seeber, J. Pacheco, *Geophys. Res. Lett.* **16**, 199 (1989).
4. J. R. Booker, *J. Geophys. Res.* **79**, 2037 (1974); C. H. Scholz, *Geology* **2**, 551 (1974); J. B. Rundle and W. Thatcher, *Bull. Seismol. Soc. Am.* **70**, 1869 (1980).
5. GPS arrays in the region of Landers have station spacing of ~10 km or more and therefore capture only long-wavelength features of the deformation field (*1*). Small-aperture trilateration arrays were surveyed after the earthquake and were able to measure only minor, localized deformation along the 1992 rupture [A. G. Sylvester, *Geophys. Res. Lett.* **20**, 1079 (1993)]. Creepmeters along the Eureka Peak fault revealed up to 23 cm of surface slip in 1 year [J. Behr *et al.*, *Bull. Seismol. Soc. Am.* **84**, 826 (1994)].
6. H. Gabriel, R. Goldstein, H. Zebker, *J. Geophys. Res.* **94**, 9183 (1989); H. Zebker *et al.*, *ibid.* **99**, 19617 (1994); G. Peltzer and P. Rosen, *Science* **268**, 1333 (1995).
7. We used the three-pass method to process SAR data acquired by the European remote sensing satellite (ERS-1) into interferograms (*6*). Each SAR image triplet forms a pair of images spanning a long time interval with a small spatial baseline (*6*) and a pair spanning a short time interval to remove the topographic phase signal. The data were acquired on descending orbits on (A) 7 August 1992–24 September 1995–11 June 1995, (B) 27 September 1992–23 January 1996–14 November 1995, and (C) 10 January 1993–23 May 1995–14 November 1995. For each image triplet, the first two dates correspond to the long time interval pair and the last two dates to the pair used to remove the topography.
8. Surface strain patterns of longer wavelength are also clear in the intermediate field and are the subject of a separate study (G. Peltzer *et al.*, in preparation).
9. K. Sieh *et al.*, *Science* **260**, 171 (1993); E. W. Hart *et al.*, *California Geol.* **46**, 10 (1993).
10. J. M. Sower *et al.*, *Bull. Seismol. Soc. Am.* **84**, 528 (1994); J. A. Spotila and K. Sieh, *J. Geophys. Res.* **100**, 545 (1995).
11. A. Sylvester, personal communication.
12. For ERS-1, the satellite line of sight is nearly perpendicular to the orbit and has an incidence angle of 23° in the center of the scene [European Space Agency, *ERS-1 System* (ESA Publications Division, ESTEC, Noordwijk, Netherlands, 1992)].
13. See, for example, K. Mogi, *Tokyo Univ. Earthquake Res. Inst. Bull.* **40**, 107 (1962); P. J. Eaton, *U.S. Geol. Surv. Prof. Pap. 579* (1967).
14. D. L. Anderson and J. H. Whitcomb, *J. Geophys. Res.* **80**, 1497 (1975); R. Muir-Wood and G. C. P. King, *J. Geophys. Res.* **98**, 22035 (1993).
15. J. K. MacKenzie [*Proc. Phys. Soc. London Sect. B* **63**, 1 (1950)] derived the elastic constants for a solid containing spherical holes, and Y. Sato [*Tokyo Univ. Earthquake Res. Inst. Bull.* **30**, 178 (1952)] extended the study to solids with holes filled with a fluid. Assuming a porosity of 2%, a Poisson's ratio of 0.27 for the solid, and the compressibility of the pore fluid to be equal to that of the solid, Sato's equations 3.2 and 3.3 give the Poisson's ratios of the drained material $\nu_d = 0.268$ and the undrained material $\nu_u = 0.278$ (note that $\nu_d < \nu_u$). These values are within the range of the values listed by J. R. Rice and M. P. Cleary [*Rev. Geophys. Space Phys.* **14**, 227 (1976)], estimated from laboratory tests for a variety of crustal materials. If the values listed for charcoal granite—which has a Poisson's ratio of 0.27, close to the ratio of 0.29 estimated from *P*-wave velocities for the upper crust in the Mojave Desert [Y. G. Li, L. T. Henyey, P. C. Leary, *J. Geophys. Res.* **97**, 8817 (1992)]—are representative of crustal materials at Landers, then $\nu_d = 0.27$ and $\nu_u = 0.30$. We assume $\nu_u - \nu_d = 0.03$ for the present calculation, although large uncertainties clearly exist for these values.
16. An alternative model involving fault collapse and fault strike perpendicular compression has been advocated to explain surface uplift near the Johnson Valley fault [D. Massonnet, W. Thatcher, H. Vadon, *Nature* **382**, 612 (1996)]. Although fault strike perpendicular compression may have actually occurred after the 1992 Landers earthquake, such a model does not explain the fact that the observed strain is localized in fault step-overs and is not distributed along the entire 1992 rupture, nor does it explain the subsidence observed in the compressive jog along the Emerson–Camp Rock fault.
17. Given a length scale of 10 km, the calculated relaxation time of 270 days yields a hydraulic diffusivity on the order of 10^4 cm^2 s^{-1}, consistent with the value estimated for a variety of earthquake-associated phenomena (*14*).

18. We thank E. Ivins and P. Segall for discussions on postseismic deformation processes, A. Sylvester for sharing unpublished results of leveling across the Homestead Valley fault, and two anonymous reviewers for constructive suggestions. The ERS-1 radar data were provided by the European Space Agency. The research described in this paper was carried out at the Jet Propulsion Laboratory, California Institute of Technology, under contract with NASA, and at the U.S. Geological Survey.

4 June 1996; accepted 17 July 1996

The Metabolic Status of Some Late Cretaceous Dinosaurs

John A. Ruben,* Willem J. Hillenius, Nicholas R. Geist, Andrew Leitch, Terry D. Jones, Philip J. Currie, John R. Horner, George Espe III

Analysis of the nasal region in fossils of three theropod dinosaurs (*Nanotyrannus, Ornithomimus,* and *Dromaeosaurus*) and one ornithischian dinosaur (*Hypacrosaurus*) showed that their metabolic rates were significantly lower than metabolic rates in modern birds and mammals. In extant endotherms and ectotherms, the cross-sectional area of the nasal passage scales approximately with increasing body mass M at $M^{0.72}$. However, the cross-sectional area of nasal passages in endotherms is approximately four times that of ectotherms. The dinosaurs studied here have narrow nasal passages that are consistent with low lung ventilation rates and the absence of respiratory turbinates.

Knowledge of dinosaur metabolic physiology can help improve understanding of their feeding and reproductive habits, as well as their routine modes of existence. Similarly, because birds are probably descendants (*1*) or near relatives of dinosaurs